nature sustainability

ARTICLES

https://doi.org/10.1038/s41893-021-00697-4

Check for updates

Selective recovery of precious metals through photocatalysis

Yao Chen[1], Mengjiao Xu[1], Jieya Wen[1], Yu Wan[1], Qingfei Zhao[1], Xia Cao[2], Yong Ding[3], Zhong Lin Wang[2,3] ✉, Hexing Li[1,4] ✉ and Zhenfeng Bian[1] ✉

Precious metals such as gold and platinum are valued materials for a variety of important applications, but their scarcity poses a risk of supply disruption. Recycling precious metals from waste provides a promising solution; however, conventional metallurgical methods bear high environmental costs and energy consumption. Here, we report a photocatalytic process that enables one to selectively retrieve seven precious metals—silver (Ag), gold (Au), palladium (Pd), platinum (Pt), rhodium (Rh), ruthenium (Ru) and iridium (Ir)—from waste circuit boards, ternary automotive catalysts and ores. The whole process does not involve strong acids or bases or toxic cyanide, but needs only light and photocatalysts such as titanium dioxide (TiO_2). More than 99% of the targeted elements in the waste sources can be dissolved and the precious metals recovered after a simple reducing reaction that shows a high purity (≥98%). By demonstrating success at the kilogram scale and showing that the catalysts can be reused more than 100 times, we suggest that this approach might be industry compatible. This research opens up a new path in the development of sustainable technologies for recycling the Earth's resources and contributing to a circular economy.

Precious metals (PMs) possess not only good physical properties (such as ductility and electrical conductivity), but also high chemical stability and strong corrosion resistance[1]. In recent years, PMs have been increasingly used in the fields of electronic devices and modern industrial catalysis[2,3]. It is reported that the global demand for gold, silver and palladium in the electronics industry was about 250 tonnes, 12,800 tonnes and 40 tonnes, respectively[4–6]. Furthermore, owing to the continuous growth of the automotive industry, the consumption of platinum-group metals is increasing[5]. By contrast, the global electronic waste (e-waste) production shows that the gold content in 40 mobile phones is equivalent to 1 tonne of ore[7]. In 2019, a total of 53.6 million tonnes of PM-containing e-waste was generated globally, including discarded computers, mobile phones and households electronic equipment[8,9]. Once an appropriate technology is developed, these wastes could become a major sustainable source for PMs.

Unfortunately, it remains a grand challenge to mine and capture PMs from ores, catalysts and e-waste[10–13]. The recovery process of PMs comprises two major steps: first, dissolution of PM^0 forming PM^{x+} solutions and then the reduction of PM^{x+} to PM^0 from the leachate. The most widely used dissolution methods in the industry involve strongly corrosive and toxic aqua regia and cyanidation and, therefore, endanger the environment[14–17]. In view of the toxicity of aqua regia and cyanide, alternative non-toxic leaching agents, such as thiourea, thiosulfate and iodine, have been developed to dissolve gold, but they are not effective for the leaching of platinum group PMs, and the reaction processes are often complicated[13,18–23] (Supplementary Table 1). Recently, Yang and colleagues[13] applied *n*-bromosuccinimide (NBS) and pyridine to directly leach Au^0 waste from gold ores and electronics to form Au(III). Hong and colleagues used sulfuryl chloride ($SOCl_2$) and organic solvents/reagents(pyridine, *N*,*N*-dimethylformamide and imidazole) as an organic form of aqua regia to dissolve gold and palladium[23]. However, these methods prove effective for only one or two PMs, and the reagent design is not favourable in terms of operation and cost. Compared with the dissolution process, reduction of PM^{x+} to PM^0 requires materials that must be resistant to harsh media such as acidic solutions, which is challenging. A recent report showed that a porous porphyrin polymer can capture PM ions from the acidic exudate of e-waste[24]. Smith and colleagues used 1,3:2,4-dibenzylidenesorbitol-derived hydrogels to extract gold and silver ions[25]. Queen and colleagues prepared Fe-BTC/PpPDA composite material, which was proven to quickly extract trace amounts of gold ions from water mixtures[11]. However, the synthesis of the leaching material and the subsequent reaction processes are very complicated.

The photocatalytic reactions are known to produce a range of highly reactive free radicals that can react with other species of interest. Moreover, photocatalysis is characterized by low energy requirements, easy operation, high efficiency and zero hazardous emissions. In light of the redox potential (normal hydrogen electrode (NHE) and reversible hydrogen electrode (RHE)) of photogenerated holes (TiO_2 (2.91 V_{NHE})), it is sufficient for them to oxidize PM^0 into PM^{x+} (Rh (0.75 V_{RHE}) < Ir (0.9 V_{RHE}) < Pt (1.1 V_{RHE}) < Au (1.3 V_{RHE}))[26,27]. As a result, photocatalytic oxidation could be the technology of choice to tackle environmental and energy issues, although reports on the oxidation and dissolution of PMs using this green approach are lacking.

In this Article, we report the use of photocatalysis to dissolve and recover a series of PMs (Ag, Au, Pd, Pt, Ru, Rh and Ir) in the absence of strong acids, strong bases and toxic solvents. Interestingly, the dissolution is selective, enabling the separation of metals of interest from others. More importantly, this photocatalytic technology applies to different waste sources, including e-waste, automotive

[1]MOE Key Laboratory of Resource Chemistry and Shanghai Key Laboratory of Rare Earth Functional Materials, Shanghai Normal University, Shanghai, China. [2]Beijing Institute of Nanoenergy and Nanosystems, Chinese Academy of Sciences, Beijing, China. [3]School of Materials Science and Engineering, Georgia Institute of Technology, Atlanta, GA, USA. [4]Shanghai University of Electric Power, Shanghai, China. ✉e-mail: zlwang@gatech.edu; hexing-li@shnu.edu.cn; bianzhenfeng@shnu.edu.cn

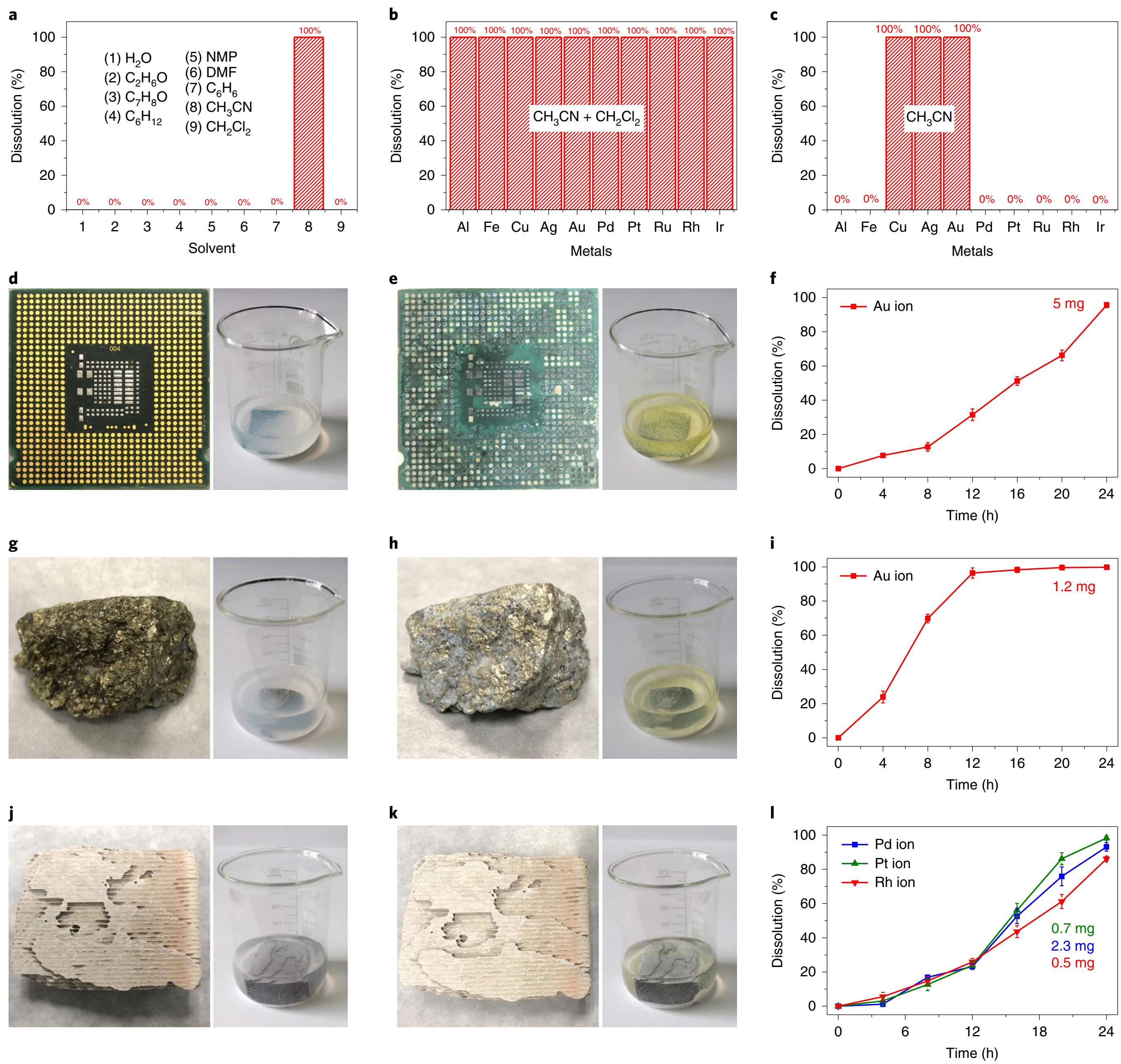

Fig. 1 | Photocatalytic dissolution of PMs. a, The dissolution percentage of Au in different solutions. **b**, The dissolution percentages of Al, Fe, Cu, Ag, Au, Pd, Pt, Ru, Rh and Ir in the mixed system of acetonitrile and DCM under photocatalytic conditions. **c**, The dissolution rate of Al, Fe, Cu, Ag, Au, Pd, Pt, Ru, Rh and Ir in acetonitrile under photocatalytic conditions. **d–l**, Photocatalytic dissolution of PMs from a CPU board, gold ore and TWC. **d**,**e**, Photographs of retrieving gold from a CPU board before (**d**) and after (**e**) the reaction. **g**,**h**, Photographs of retrieving gold from gold ore (28.8 g) before (**g**) and after (**h**) the reaction. **j**,**k**, Photographs of retrieving PMs from TWC (17.9 g) before (**j**) and after (**k**) the reaction. **f**,**i**,**l**, The amount of PMs obtained by photocatalysing an unbroken CPU board (**f**), gold ore (**i**) and TWC (**l**).

three-way catalysts and ores, and can function effectively on a large scale (kilograms). This research potentially offers a sustainable and affordable approach to the recovery of PMs and is expected to inspire more efforts into the advancement of technologies for resource recycling.

Results

Here, photocatalysis is used to extract PMs from waste central processing unit (CPU) boards, three-way catalysts (TWC) and ore. We started by screening a list of solvents that are commonly used to dissolve PMs, confirming that acetonitrile (MeCN) is the best choice (Fig. 1a). Our results show that Au could be completely dissolved into MeCN, whereas other solvents show no uptake at all. Mixing MeCN with dichloromethane (DCM) could optimize the variety of metals to be leached. Remarkably, it was found that seven different PMs (Au, Ag, Pd, Pt, Ru, Rh and Ir) and three common participating non-precious elements in e-waste (Fe, Al and Cu) can be fully dissolved in the mixture solution (Fig. 1b and Supplementary Fig. 1). By contrast, only Au, Ag and Cu could be captured if MeCN is used as a single solvent (Fig. 1c).

As shown in Supplementary Fig. 2, simply soaking the waste and TiO_2 powders in the mixed MeCN–DCM solvent and exposing them to light irradiation, Au present in CPU board (Fig. 1d) and gold ore (28.8 g; Fig. 1g), as well as several PMs contained in TWC (17.9 g)—including Pd, Pt and Rh (Fig. 1j), all of which can be leached—forms solutions with different colours (Fig. 1e,h,k). The reaction takes place under ambient temperature and pressure, and may need 1–24 h depending on the depth of leaching. After 24 h, around 5 mg and 1.2 mg Au from one piece of CPU board sample and 28.8 g ore, respectively, could be extracted (Fig. 1f,i). In the case of TWC, up to 0.7 mg Pt, 2.3 mg Pd and 0.5 mg Rh were dissolved into the solution (Fig. 1l). Unsurprisingly, crushing the bulk waste samples to scraps could increase the surface area of contact of the reactants and therefore accelerate the reaction and help to dissolve more metals (Supplementary Fig. 3). Some other elements such as Cu, Ni and Ag are present in the CPU board (Supplementary Fig. 4) and they can also be leached (Supplementary Fig. 5). Note that the present reaction is mild compared with aqua regia, which reacts vigorously, producing toxic gases, such as NO and chlorine, and cracking the CPU board (Supplementary Fig. 6).

Selective and scalable dissolution of PMs. The e-waste, TWC and ore usually contain a variety of metals. Ideally, a PM should be leached selectively in the presence of competing metal species. To evaluate the selectivity, a photocatalytic dissolution test was performed on TiO_2 samples loaded with four of the most widely used metals, including Cu, Ag, Au and Pt. As shown in Fig. 2a,b, Cu, Ag and Au were dissolved sequentially in MeCN over the course of the reaction before DCM was introduced to enable the dissolution of Pt, demonstrating that the present photocatalytic approach is selective. As a result, when CPU board was treated, the elements that were present, including Cu, Ag and Au, could be leached one by one with increasing irradiation time (Fig. 2c,d and Supplementary Table 2). The selectivity is rooted in the reactivity of the metals (Cu > Ag > Au), whereby the dissolution of Cu takes priority over Ag and Au. Otherwise, Ag and Au ions will be reduced by Cu metals. Furthermore, as the concentration of Cu is much higher than that of Ag and Au in the CPU board, the full dissolution of Cu took more time (8 h) compared with for Ag (4 h) and Au (another 4 h; Supplementary Table 3). We noted that the Ni on the CPU board cannot be adsorbed in MeCN (Supplementary Fig. 7). This shows that base metals and PMs can be selectively dissolved and separated. We further prepared Fe–Au alloy to assess the selectivity of photocatalytic dissolution (Supplementary Fig. 8a). It is obvious that only Au can be dissolved (100%) in MeCN without uptake of Fe (Supplementary Fig. 8b). In the case of e-waste, which contains Fe, Ni, Cu, Ag, Au and Pd, similarly selective recovery of Ag, Au and Pd can be realized by adjusting the solvent and reaction time (Fig. 2e,f). First, e-waste is soaked in dilute hydrochloric acid to remove Fe and Ni, and Cu, Ag and Au are then dissolved in MeCN by photocatalysis. Finally, Pd is dissolved in mixed MeCN and DCM.

The photocatalytic dissolution process is not only simple to be implemented but also scalable. We have further designed a reactor that is suitable for dissolution on a larger scale (Supplementary Fig. 9). With this, we are able to treat 1.137 kg of CPU board and 1.169 kg of gold ore (Fig. 2g–l). As the photocatalytic reaction proceeds, the gold on the CPU board and the ore continues to be dissolved. In 24 h, 18.3 mg and 26.1 mg of Au were dissolved from the CPU board and the ore, respectively. After 48 h, 32.5 mg and 65.9 mg of Au were captured, respectively.

Reaction kinetics. Several parameters affect the dissolution rate of the PM-leaching process, such as solvent ratio, PM content and rotation rate. An examination of Pt dissolution provided information regarding the kinetics of the present photocatalytic process, which is a fluid–solid heterogeneous reaction and is commonly described by the shrinking-nucleus model[28,29]:

$$k_c t = 1 - (1 - x)^{1/3} \quad (1)$$

where x is the leaching fraction of Pt, k_c represents the apparent rate constants (h^{-1}) for diffusion through the product layer chemical reaction and t is the reaction time. The dissolution fractions of Pt (x) were calculated according to the following equation:

$$x = M_t/M_0 \times 100\% \quad (2)$$

where M_0 is the mass of Pt in the Pt/C and M_t is the mass of Pt in the leached solution.

At a MeCN:DCM ratio of 3:1, most Pt nanoparticles (NPs) could be dissolved (Supplementary Fig. 10a). Following equation (1), the k_c could be determined and we found that the k_c could be enhanced by 1.8× and 6.4× for the ratios 1:1 and 1:3, respectively (Supplementary Fig. 10d). The leaching curve of Pt under different stirring rates is shown in Supplementary Fig. 10b,e. The results show that, when the rotating speed exceeded 600 rotations per min, the leaching rate was not affected. The larger the platinum content in the sample, the longer the leaching time that was needed, but it did not affect the leaching rate (Supplementary Fig. 10c,f).

Recovery of PMs. The dissolution solutions contain immobilized PM^{x+} ions that must be further separated and reduced to retrieve PMs. Before doing so, the solution was first filtered and evaporated to recycle the solvent (Fig. 3a–d). The obtained products were then calcined in a tube furnace at 500 °C for 2 h under a H_2 atmosphere, yielding different NPs (Supplementary Fig. 11b). The corresponding powder X-ray diffraction (XRD) patterns show the characteristic peaks for Ag, Au, Pt and Pd metals (Fig. 3e–h). Scanning electron microscopy (SEM) images indicate that the PMs are NPs (Fig. 3i–l). Elemental analysis then confirmed the chemical composition of each sample and that the purity is higher than 98% (Fig. 3m,n).

Quantum yield. Taking the amount of consumed photon energy and dissolved and recycled PMs into account, we determined the quantum yield of photodissolution reactions in MeCN and mixed MeCN–DCM solvents (Supplementary Fig. 12). The maximum value of the incident photon-to-electron conversion efficiency (IPCE) spectra appears at ~360 nm. The apparent quantum efficiency (AQE) of the Au–MeCN system reached 0.053% at 360 nm under the optimized dissolution conditions. The AQE of the Au–MeCN–DCM system reached 0.056% at 360 nm under the optimized dissolution conditions.

Discussion

The remarkably high uptake and selectivity for PMs prompted us to understand the mechanism of the photocatalytic dissolution and reduction process. A control experiment was performed using a commercial 5% Pt/C catalyst. As shown in Fig. 4a and Supplementary Fig. 13, Pt NPs are completely dissolved after 4 h of illumination with ultraviolet light (Fig. 4b). There is no redox peak before the reaction starts (Supplementary Fig. 14). As the reaction continues, the corresponding peak to Pt ions grows gradually, confirming that Pt is progressively dissolved into the solution and consistent with X-ray photoelectron spectroscopy (XPS) spectra in which the binding energies of Pt^0 4*f* drops substantially[30] (Fig. 4c).

To reveal the structure of the solid product after solvent evaporation (Supplementary Fig. 15a), the infrared spectrum was collected, showing a different feature that was not observed for the sample in solution. As shown in Fig. 4d, the new infrared absorption peak appeared in the region of 3,344–2,913 cm^{-1}, which is a typical N–H stretching vibration peak[31]. Moreover, the original

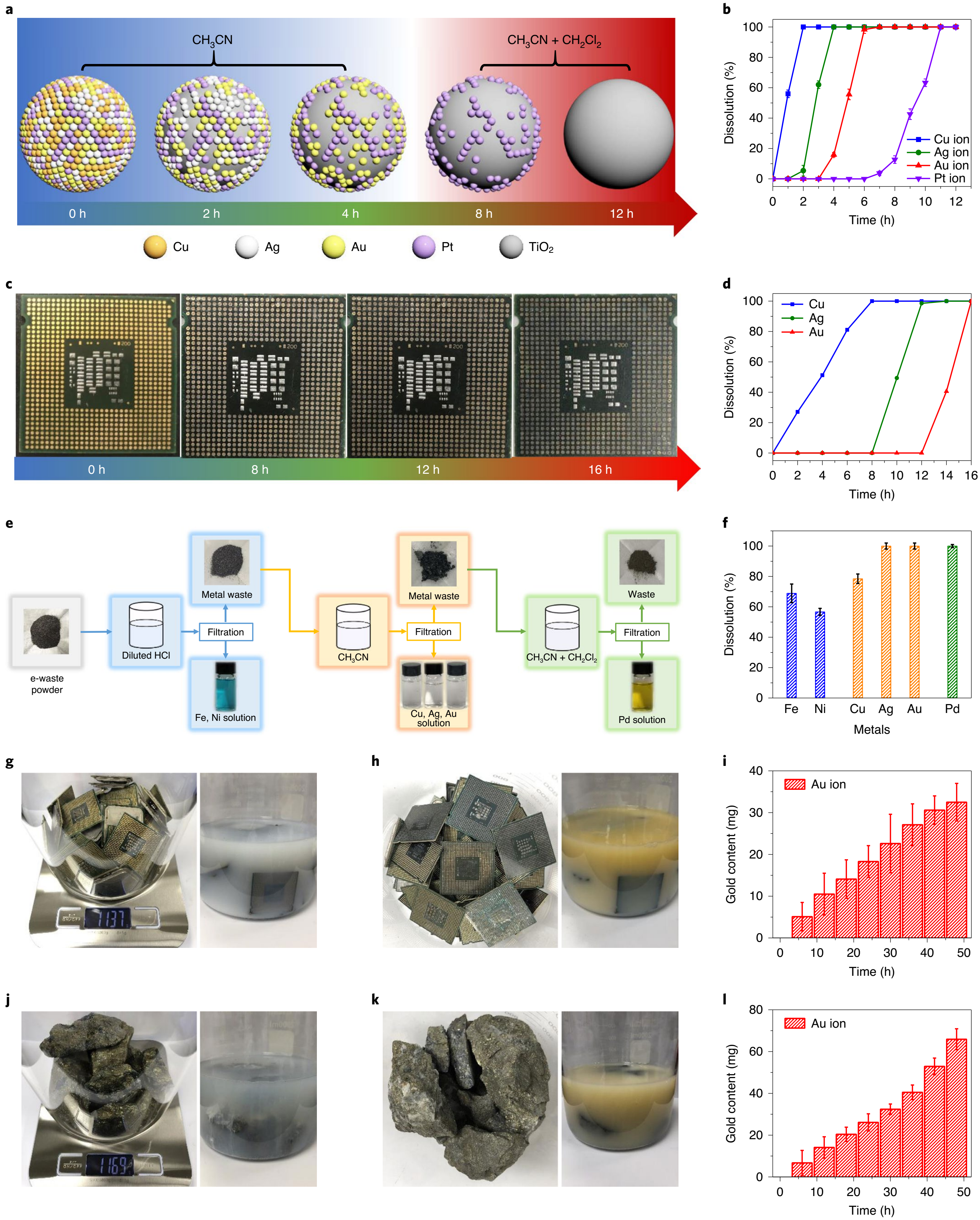

Fig. 2 | Photocatalytic selective dissolution of metals from metal catalysts (1% Cu/TiO_2, 1% Ag/TiO_2, 1% Au/TiO_2 and 1% Pt/TiO_2), CPU boards and e-waste powder. a, Schematic of the selective dissolution process of metal catalysts. **c**, Photographs of selectively retrieving metal from a CPU board. **e**, Flow sheet of the stepwise extraction of Fe, Ni, Cu, Ag, Au and Pd from e-waste powder. **g**,**h**, Photographs of retrieving gold from a CPU board (1.137 kg) before (**g**) and after (**h**) the reaction. **j**,**k**, Photographs of retrieving gold from ore (1.169 kg) before (**j**) and after (**k**) the reaction. **b**,**d**,**f**,**i**,**l**, The amount of metals obtained by selective photocatalysing metal catalysts (**b**), a single CPU (**d**), multiple CPUs (**i**), e-waste powder (**f**) and ore (**l**).

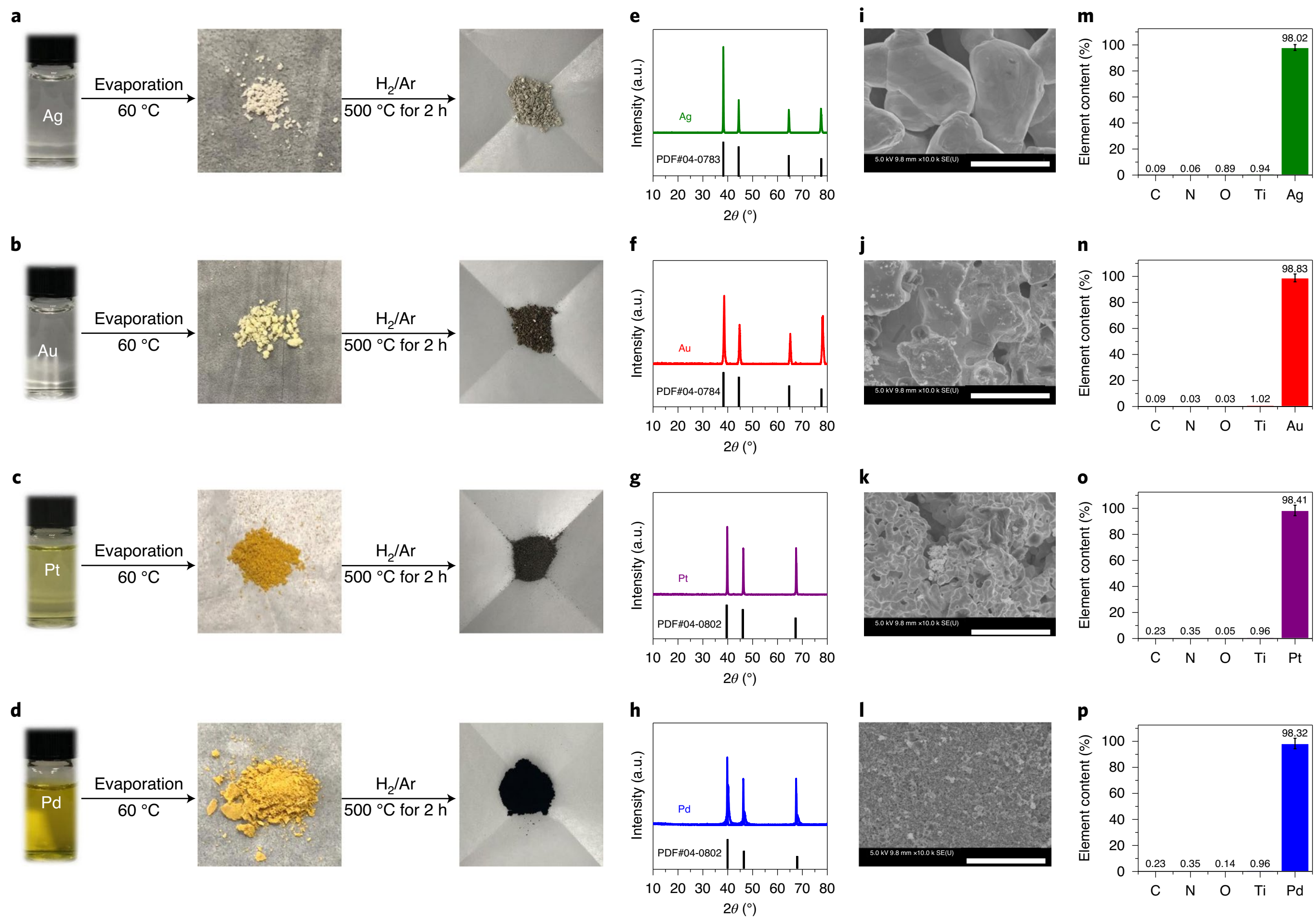

Fig. 3 | Reduction process of PM ions. a–d, The solvent of the dissolved product is removed and then calcined in a reducing atmosphere to obtain the metals Ag (**a**), Au (**b**), Pt (**c**) and Pd (**d**). **e–h**, XRD pattern of the reduced products Ag (**e**), Au (**f**), Pt (**g**) and Pd (**h**). **i–l**, SEM image of the reduced products Ag (**i**), Au (**j**), Pt (**k**) and Pd (**l**). **m–p**, The proportion of metal elements in the Ag (**m**), Au (**n**), Pt (**o**) and Pd (**p**) after calcination. For **i–l**, scale bars, 5 μm.

C–N peak vanished, suggesting that a new phase was formed during the dissolution process[32]. XRD analysis showed a pattern matching that of hexachloroplatinate ($(NH_4)_2PtCl_6$) (PDF#07-0218; XRD crystal powder diffraction JCPDS standard card (07-0218), used to determine the crystal structure) (Fig. 4e). EDS mapping and XPS analysis demonstrated that three elements (N, Cl, Pt) are present (Supplementary Fig. 16) and Pt takes both tetravalent and divalent forms, Pt^{4+} (75.3 eV and 78.6 eV) and Pt^{2+} (73.4 eV and 76.7 eV)[33,34] (Fig. 4f). The N and Cl elements also exhibit corresponding peaks of N–H and Pt–Cl (Supplementary Fig. 17). Apparently, the obtained solid is $(NH_4)_2PtCl_6$, as further evidenced by the similar colour with a commercial sample (Supplementary Fig. 15b–c). As a result, the N–H peak in the infrared spectrum should come from the amino vibration.

Furthermore, the control experiments indicate that the presence of oxygen, ultraviolet light and photocatalyst are all inevitable for Pt NP dissolution (Fig. 4g). According to the dissolution efficiency of capturing electrons (the superoxide radicals ($O_2^{\bullet-}$) formed by the combination with oxygen) and holes (Fig. 4h), the photogenerated electrons and holes are the main active charge carriers. Furthermore, electron spin resonance spectroscopy (ESR) was used to detect the species that were generated during the reaction. Compared with a blanket test in which no free radical could be observed (Supplementary Fig. 18a), the ESR spectra in Supplementary Fig. 18b evidence the formation of $O_2^{\bullet-}$ and methyl radicals ($CH_2R^{\bullet}$) under irradiation. Furthermore, the absence of hydrogen peroxide (H_2O_2) was confirmed using the iodometric method, excluding the possibility that the superoxide radical could turn to H_2O_2 (Supplementary Fig. 19). Nor do gas chromatography–mass spectrometry spectra suggest that any of the by-products are in the gas phase (Supplementary Fig. 20). The experiments of discoloured silica gel were used to prove that there was water in the solution after the reaction, and the water content in the dissolution reaction was quantitatively detected using Karl Fischer analysis. (Supplementary Fig. 21).

On the basis of these results, we were able to decode the reaction process (Fig. 4i, proposed schematic mechanism). After ultraviolet light excites TiO_2 to generate electrons and holes (stage 1), the photogenerated electrons react with O_2 molecules to form $O_2^{\bullet-}$, while holes react with MeCN in mixed solvents to deprotonate $CHCN^{\bullet}$ radicals (stage 2)[35,36]. Meanwhile, DCM is decomposed into oxidizing $CH_2Cl^{\bullet}$ (stage 3). These active species work synergistically to oxidize PM^0 to PM^{x+} (stage 4) form $(NH_4)_xPMCl_y$ solids (stage 5). This mechanism applies to the cases of Cu and Au when $(NH_4)_xCuCl_y{\cdot}2H_2O$ (Supplementary Fig. 22a) and $(NH_4)_xAuCl_y$ (Supplementary Fig. 22b) are obtained. After dissolution, both Cu and Au are oxidized to ions (Supplementary Fig. 22c,d). Here, it is oxygen rather than PM ions that deprives electrons of the ability to generate active species in a mixed solvent of MeCN and DCM. This is because oxygen is generally more easily adsorbed onto the surface of the semiconductor to occupy the sites at which PM ions are reduced[37]. Furthermore,

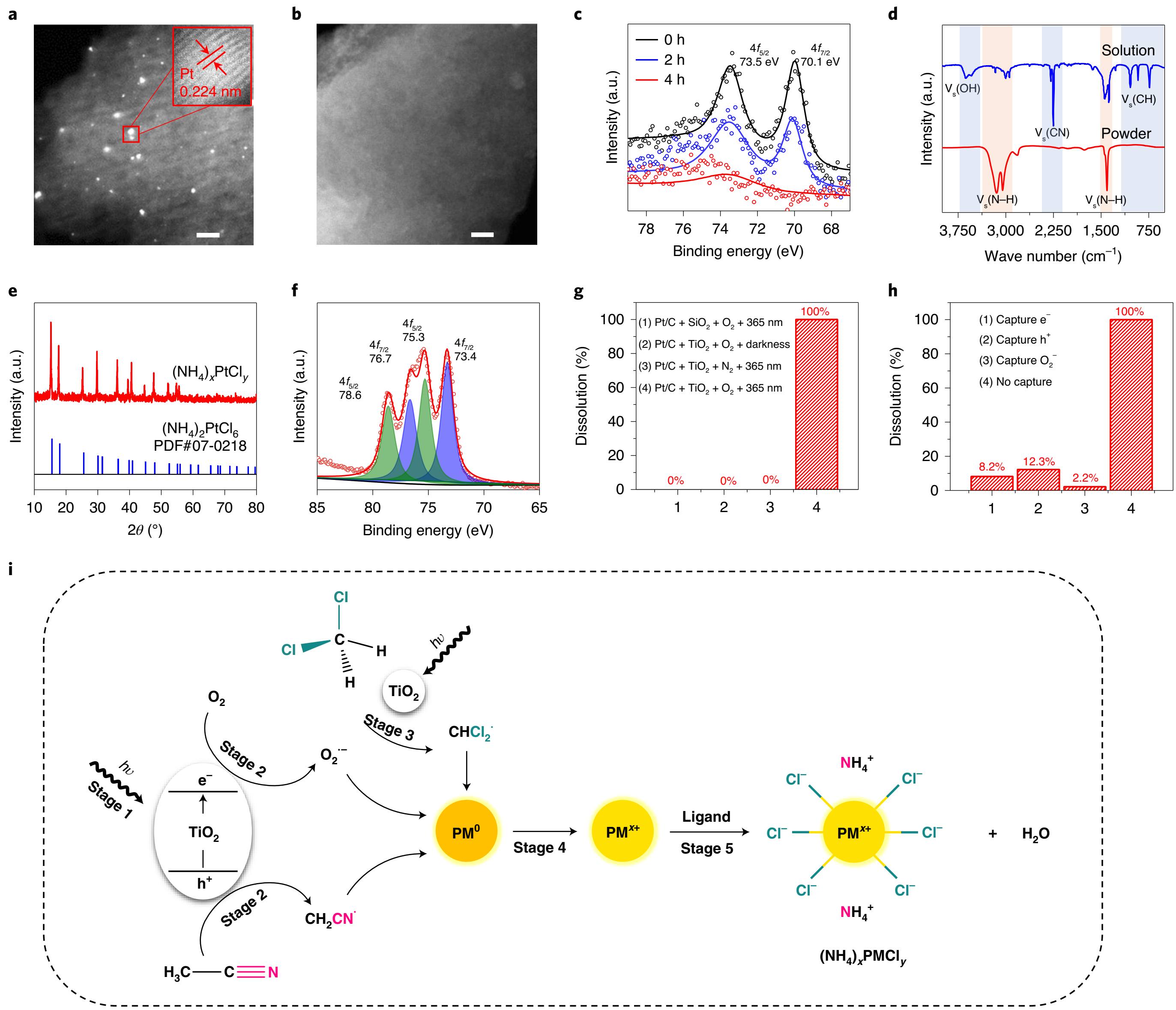

Fig. 4 | Proposed mechanism of PM recovery. a,**b**, High-angle annular dark-field scanning transmission electron microscopy images of 5% Pt/C before (**a**) and after (**b**) the reaction. The inset in **a** shows the well-resolved Pt (0.224 nm) crystalline lattices. Scale bars, 50 nm. **c**, The Pt element distribution in the Pt/C sample determined by XPS spectra with reaction time. **d**, Fourier transform infrared spectra of the solution and powder sample after the reaction. V_s, stretching vibration. **e**,**f**, XRD patterns (**e**) and Pt 4*f*7 XPS spectra (**f**) of Pt compound obtained from the solution. **g**, The dissolution percentage of Pt under different conditions. **h**, The dissolution percentage of Pt under the capture of different living species (DDQ capture electrons (e^-), EDTA-2Na capture holes (h^+), *p*-benzoquinone capture superoxide radical ($O_2^{\bullet-}$)). **i**, Proposed chemical mechanism for retrieving PMs by photocatalysis. *hυ*, light illumination.

there are differences in the activation of oxygen molecules in different solvents[38].

It is worth mentioning that the choice of supports for Pt NPs could be extended to SiO_2, Al_2O_3 and a molecular sieve (Supplementary Fig. 23). The photocatalytic approach can be extended to other photocatalysts, such as ZnO (under ultraviolet-light irradiation) or cadmium sulfide, which uses visible light without compromising the performance too much (Supplementary Fig. 24). Moreover, the importance of the cyano group and chloric substituent are notable for the selection of dissolving solvents. Organics containing -C≡N and -Cl functional groups can promote the dissolution reaction, while organics containing only -NH_x functional groups cannot initiate the dissolution of Pt (Supplementary Fig. 25). The aqueous solution of ammonium chloride cannot dissolve Pt through photocatalytic technology, and the inorganic chloride is also ineffective for the dissolution of Pt (Supplementary Fig. 26).

For a technoeconomic analysis of our recovery method, a tabulation of the costs of all of the reagents is provided in Supplementary Table 4. Here it must be pointed out that the dissolution solvent used in this research can be reused for more than 45 times (Supplementary Fig. 27). The photocatalyst can be recycled at least 100 times (Supplementary Fig. 28a) with neither morphology nor structure changed after reaction (Supplementary Figs. 28b and 28c), as well as leaving no Ti in the solution (Supplementary Fig. 28d). Without taking the recyclability into account, we estimate that the cost of photocatalytic dissolution is US$0.016 for each gram of Pt. By contrast, it will take US$0.069 to recover the same amount of Pt if aqua regia is used.

In summary, taking advantage of photocatalytic oxidation, we show a more sustainable process that features highly selective dissolution of PMs from different waste sources under ambient conditions. A high leaching efficiency of 99% is achieved for e-waste, TWC and ore, and the recycled metals show high purity. The method is simple, more environmentally friendly, scalable and is suitable for a wide range of PMs. The subsequent optimization of this work can focus on how to use water instead of organic solvents. The present solvent selection is acetonitrile and DCM, although it is a new method to avoid strong acids and cyanide. To further enhance its sustainability, water as a solvent is the best choice.

Methods

Chemicals and materials. Titanium oxide (commercial sample of Degussa P-25), 2,3-dicyano-5,6-dichlorobenzoquinone (98%), ethylenediaminetetraacetic acid disodium salt (98%), *p*-benzoquinone (99%), aluminium oxide (α phase, 99.99% metal basis, 30 nm), silicon dioxide (99.99% metal basis, 5 μm), 4 Å molecular sieve (4–8 mesh), carbon nanotube (≥95%, <2 nm, 0.3–5 μm), zinc oxide (99.9% metal basis, 30 ± 10 nm), gold chloride trihydrate (≥99.9% trace metal basis), chloroplatinic acid hexahydrate (Pt ≥ 37.5%), allochroic silicagel (2–5 mm), palladium chloride (Pd ≥ 59.8%), silver nitrate (analytical reagent (AR), 99.8%), cupric nitrate trihydrate (AR, 99%), ethanol (AR, $H_2O \leq 0.3\%$), sodium borohydride (98%), ammonium chloride (AR, 99.5%), sodium chloride (99.99% metal basis), potassium chloride (≥99.99% metal basis), 5,5-dimethyl-1-pyrroline *N*-oxide (97%) were purchased from Aladdin (AR). Cadmium sulfide (CdS) was prepared using a typical method[39]. All of the commercial catalysts (5% Pt/C, 5% Pd/C, 5% Ru/C, 5% Rh/C and 5% Ir/C), aluminium (reagent grade (RG), 99.95%, 25 μm), iron (RG, 99.99%), copper (RG, 99.99%), ammonium chloroplatinate (RG, 98%+), hydrochloric acid (37%), nitric acid (69%), potassium bromide (99.99%), gold foil (99%), lithium chloride (99.99%) used in this study were purchased from Adamas-beta (SBU). All of the solvents (acetonitrile (99.9%), DCM (99.5%), ethanol (99.9%), benzyl alcohol (99%), acetone (99.9%), benzene (99%), *N*-methyl pyrrolidone (≥99.0%), *N*,*N*-dimethylformamide (≥99.5%), hexamethylene (≥99.5%), trichloromethane (99.8%), tetrachloromethane (99.5%), 2-chlorobenzaldehyde (99%), 2,2,2-trichloroethanol (98%), triethanolamine (99%)) used in this study were purchased from Adamas-beta (RG). CPUs, ore, TWC and dismantled factory waste machines were purchased from Alibaba. Fe–Au alloy was prepared using a typical method[40]. All of the chemicals were used as received.

Synthesis of Pt NPs. Pt NPs were prepared using a typical reduction method[41]. $H_2PtCl_6 \cdot 6H_2O$ aqueous solution (2 ml of 10 mg ml^{-1}) was dispersed in 10 ml of deionized water, and 1.8 g of cetrimonium bromide was dissolved therein. After thoroughly stirring and dissolving at 50 °C, the temperature was raised to 60 °C. Then, 6.5 ml of 0.01 M NaBH was quickly added to the stirred solution and the colour change of the solution was then observed. When the solution turned brown, it was reacted for another 5 min. The resulting solution was the Pt NPs and was stored at room temperature.

Synthesis of Au NPs. Au NPs were synthesized according to the method developed by Frens[42]. In brief, 1 ml of 10 mM chloroauric acid was added to 100 ml of deionized water, and the solution was boiled. Next, 5.0 ml of 1 M trisodium citrate was added to the solution to obtain AuNPs. The solution was refluxed until a colour change from dark blue to red.

Synthesis of Ag NPs. Ag NPs were prepared using a typical reduction method[43]. A solution of 5×10^{-3} M $AgNO_3$ (100 ml) was added portionwise to 300 ml of vigorously stirred ice-cold 2×10^{-3} M $NaBH_4$. A solution of 1% poly(vinyl) alcohol (50 ml) was added during the reduction. The mixture was then boiled for around 1 h to decompose any excess of $NaBH_4$. The final volume was adjusted to 500 ml.

Synthesis of Pt/TiO_2, Ag/TiO_2, Au/TiO_2, 5% Ag/C and 5% Au/C. A certain amount of TiO_2 (Degussa P25) was placed in a solution of the prepared Pt NPs. After stirring for 2 h, the colour of the powder changed from white to light brown. The Pt/TiO_2 sample in the reactor was collected by centrifugation and washed several times with water and ethanol, and dried overnight at 80 °C. Samples of 1% Pt/SiO_2, 1% Pt/Al_2O_3 and 1% Pt/4 Å molecular sieves were synthesized using the same method, whereby TiO_2 was replaced by SiO_2, Al_2O_3 and 4 Å molecular sieves. Samples of 1% Ag/TiO_2 and 1% Au/TiO_2 were synthesized using the same method, whereby Pt NPs were replaced by Ag NPs or Au NPs. Samples of 5% Ag/C and 5% Au/C were synthesized using the same method, whereby TiO_2 was replaced by C and Pt NPs were replaced by Ag NPs or Au NPs.

Synthesis of Cu/TiO_2. Cu/TiO_2 was prepared by a simple precipitation method[44]. In brief, 0.5 g of TiO_2 (Degussa P25) was dispersed in NaOH aqueous solution, and then a certain volume of $CuCl_2$ solution was added dropwise under stirring. After further stirring for 6 h, the precipitates were washed with deionized water until pH 7, and then dried at 80 °C for 12 h. Finally, Cu/TiO_2 was calcined at 400 °C for 2 h in nitrogen. Samples of 1% Cu/SiO_2 were synthesized using the same method, in which TiO_2 was replaced by SiO_2.

Photocatalytic dissolution of PMs from CPU, ore and TWC. At 20 °C, an amount of CPU, gold ore or TWC was placed into a mixed solution of 50 ml MeCN and DCM (3:1). Next, 50 mg TiO_2 was added directly into the solution. For the dissolution of 1 kg of CPUs and ore, 500 ml of a mixture of MeCN and DCM (3:1) and 500 mg of TiO_2 was added. Ultraviolet-light irradiation (100 W 365 nm LED lamp, Beijing Perfectlight) was then applied to the mixed solution for 50 h. The dissolution was calculated by measuring the concentration of PM in the solution using inductively coupled plasma emission spectrometry (ICP, Jarrel-Asm Atom Scan 2000).

Selective dissolution of metal NPs. The metal-selective dissolution properties of the system were tested by photocatalytic induction of commercial metals catalyst (5% Ag/C, 5% Au/C, 5% Pt/C, 5% Pd/C, 5% Ru/C, 5% Rh/C and 5% Ir/C, Al (RG, 99.95%, 25 μm), Fe (RG, 99.99%) and Cu (RG, 99.99%)). Typically, 50 mg of commercial metal catalyst and 50 mg TiO_2 were dispersed in MeCN or a mixture of MeCN and DCM (3:1) (20 ml) and irradiated with a 100 W 365 nm LED lamp (15 mW m^{-2}) at 20 °C. In the comparative experiment, the selective dissolution of gold was explored by replacing solvents with water (H_2O), ethanol (C_2H_6O), acetone (C_7H_8O), benzene (C_6H_{12}), cyclohexane (C_6H_6), dimethyl formamide, *N*-methyl pyrrolidone and DCM (CH_2Cl_2). The degree of dissolution was calculated by measuring the concentration of platinum in the solution during the dissolution process using ICP (Jarrel-Asm Atom Scan 2000).

Selective dissolution of PMs from CPU and metal catalyst. At 20 °C, a piece of CPU was placed into 50 ml acetonitrile solution. Next, 50 mg TiO_2 was directly added into the solution. Then ultraviolet-light irradiation was applied to the mixed solution for a certain time. An amount of 1% Cu/TiO_2 (50 mg), 1% Ag/TiO_2 (50 mg), 1% Au/TiO_2 (50 mg) and 1% Pt/TiO_2 (50 mg) was placed into a 15 ml acetonitrile solution. Next, ultraviolet-light irradiation was applied to the mixed solution for a certain time. First, copper, silver and gold were completely dissolved after 6 h. Then, the undissolved residual solid was centrifuged and placed into a mixed solvent of acetonitrile and DCM, which can dissolve platinum.

Selective dissolution of PMs from e-waste powder. First, we immersed e-waste powder (1 g) in 50 ml diluted hydrochloric acid (HCl, 1 M) and reacted for 5 h to remove some non-PMs (such as Fe and Ni). Second, the undissolved sample was separated and washed, and then put into the MeCN solution (50 ml). Next, 100 mg TiO_2 was added directly into the solution. Ultraviolet-light irradiation was then applied to the mixed solution for a certain time. Finally, the undissolved sample was separated and washed, and then put into the mixed solution of MeCN and DCM (3:1, 50 ml). Next, 100 mg TiO_2 was added into the above solution, and then ultraviolet-light irradiation was applied to the mixed solution for a certain period of time. The dissolution was calculated by measuring the concentration of PM in the solution using ICP (Jarrel-Asm Atom Scan 2000).

Dissolution of platinum NPs. At 20 °C, the PM-dissolution properties of the system were tested by photocatalytic induction of a platinum catalyst (5% Pt/C). Typically, 50 mg of 5% Pt/C catalyst and 50 mg TiO_2 were dispersed into a mixed solution of 20 ml MeCN and DCM (3:1) and irradiated with a 100 W 365 nm LED lamp (15 mW m^{-2}). Control experiments were conducted under the conditions of darkness, nitrogen atmosphere or SiO_2 as a catalyst. The degree of dissolution was calculated by measuring the concentration of platinum in the solution during the dissolution process using ICP (Jarrel-Asm Atom Scan 2000).

Calculating the dissolution rate. Owing to the volatilization of chlorine in the aqua regia, we put the reacted sample in the aqua regia into a fume hood and reacted for 5 h such that the remaining PMs on the sample were completely leached. Then, the photocatalytic dissolution efficiency was calculated according to the remaining metal content, and the dissolution rate was calculated according to the equation below:

$$\text{Dissolution rate } (\%) = \frac{\text{The amount of PM leaching by photocatalytic dissolution } (\text{mg l}^{-1})}{\text{The amount of PM leaching by aqua regia } (\text{mg l}^{-1})} \times 100 \quad (3)$$

As silver and rhodium cannot be dissolved in aqua regia, silver and rhodium were dissolved in concentrated nitric acid and hydrofluoric acid, respectively.

PM ion reduction process. The leachate was recovered after distillation at a low temperature (60 °C), and the solid product was calcined and reduced under an H_2/Ar atmosphere at 500 °C.

Calculating AQE. The AQE at each centred wavelength of the monochromatic light was calculated from the ratio of the number of PM dissolution to those of the irradiated photons using the following expression:

$$\text{AQE} = \frac{\text{Number of PM dissolution}}{\text{Number of incident photons}} \times 100\% \quad (4)$$

Characterization. The dissolution was calculated by measuring the concentration of PM in the solution using ICP (Jarrel-Asm Atom Scan 2000). The catalyst samples were characterized using scanning transmission electron microscopy (STEM) (high-angle annular dark-field STEM, FEI G2 Tecnai F20, 200 kV and JEOL ARM200F with a probe corrector), XPS (PerkinElmer PHI 5000C, Al Kα), UV-VIS diffuse reflectance spectra (Shimadzu, UV2600). The ESR spectra of the transition metal in the solution were recorded using the JEOL JES-FA200 model spectrometer to estimate the valence composition of platinum. The solution samples after reaction were characterized using Fourier transform infrared spectrometry (Nicolet IS 10). Powder samples (obtained by evaporating the reacted solution under low temperature) were characterized using field emission SEM (HITACHI S4800, operated at 50 kV), Fourier transform infrared spectrometry (Nicolet Nexus 470), XPS (PerkinElmer PHI 5000C, Al Kα) and XRD (Rigaku D/MAX-2000). All of the binding energies were calibrated using the contaminant carbon (C1*s* = 284.8 eV) as a reference. Gas compositions were measured using GC–MS (GCMS-QP2010, Shimadzu). The GC system was equipped with a SH-Rxi-5Sil-fused silica capillary column. Quantitative detection of water content in the dissolution reaction was performed using Karl Fischer analysis (870 KF Titrino plus). Photoelectrochemical measurements were performed in a conventional three-electrode, single-compartment quartz cell on an electrochemical station (CHI 660D). A bias voltage of 0.5 V was used to drive the transfer of photogenerated electrons from the working electrode to the platinum electrode. A LiCl acetonitrile or mixed solution (0.50 M) was used as the electrolyte.

Reporting Summary. Further information on research design is available in the Nature Research Reporting Summary linked to this article.

Data availability

The data supporting the findings of the study are available within the paper and its Supplementary Information.

Received: 25 February 2020; Accepted: 11 February 2021;
Published online: 25 March 2021

References

1. Fan, Z. & Zhang, H. Crystal phase-controlled synthesis, properties and applications of noble metal nanomaterials. *Chem. Soc. Rev.* **45**, 63–82 (2016).
2. Zhao, M. et al. Metal-organic frameworks as selectivity regulators for hydrogenation reactions. *Nature* **539**, 76–80 (2016).
3. Hunt, S. T. et al. Self-assembly of noble metal monolayers on transition metal carbide nanoparticle catalysts. *Science* **352**, 947–978 (2019).
4. *Commodity Statistics and Information* (USGS, 2017); https://minerals.usgs.gov/minerals/pubs/commodity/
5. Li, B. et al. Recovery of platinum group metals from spent catalysts: a review. *Int. J. Miner. Process.* **145**, 108–113 (2015).
6. *Annual Consumption and Storage of Metals in the World* (NIMS, 2015); http://www.nims.go.jp/jpn/news/press/pdf/press215_2.pdf
7. Yavuz, C. T. et al. Gold recovery from e-waste by porous porphyrin–phenazine network polymers. *Chem. Mater.* **32**, 5343–5349 (2020).
8. Liu, C. et al. Economic and environmental feasibility of hydrometallurgical process for recycling waste mobile phones. *Waste Manag.* **111**, 41–50 (2020).
9. Dato, P. Economic analysis of e-waste market. *Int. Environ. Agreem.* **17**, 815–837 (2017).
10. Doidge, E. D. et al. A simple primary amide for the selective recovery of gold from secondary resources. *Angew. Chem. Int. Ed.* **55**, 12436–12439 (2016).
11. Sun, D. T., Gasilova, N., Yang, S., Oveisi, E. & Queen, W. L. Rapid, selective extraction of rrace amounts of gold from complex water mixtures with a metal-organic framework (MOF)/polymer composite. *J. Am. Chem. Soc.* **140**, 16697–16703 (2018).
12. Liu, Z. et al. Selective isolation of gold facilitated by second-sphere coordination with alpha-cyclodextrin. *Nat. Commun.* **4**, 1855 (2013).
13. Yue, C. et al. Environmentally benign, rapid, and selective extraction of gold from ores and waste electronic materials. *Angew. Chem. Int. Ed.* **56**, 9331–9335 (2017).
14. McGivney, E. et al. Biogenic cyanide production promotes dissolution of gold nanoparticles in soil. *Environ. Sci. Technol.* **53**, 1287–1295 (2019).
15. Birich, A., Stopic, S. & Friedrich, B. Kinetic investigation and dissolution behavior of cyanide alternative gold leaching reagents. *Sci. Rep.* **9**, 7191 (2019).
16. Ahtiainen, R. & Lundström, M. Cyanide-free gold leaching in exceptionally mild chloride solutions. *J. Clean. Prod.* **234**, 9–17 (2019).
17. James Hutton: father of modern geology, 1726–1797. *Nature* **119**, 582 (1927).
18. Lee, H., Molstad, E. & Mishra, B. Recovery of gold and silver from secondary sources of electronic waste processing by thiourea leaching. *JOM* **70**, 1616–1621 (2018).
19. Burdinski, D. & Blees, M. H. Thiosulfate- and thiosulfonate-based etchants for the patterning of gold using microcontact printing. *Chem. Mater.* **19**, 3933–3944 (2007).
20. Cho, E. C., Xie, J., Wurm, P. A. & Xia, Y. Understanding the role of surface charges in cellular adsorption versus internalization by selectively removing gold nanoparticles on the cell surface with a I_2/KI etchant. *Nano Lett.* **9**, 1080–1084 (2009).
21. Parga, J. R., Valenzuela, J. L. & Francisco, C. T. Pressure cyanide leaching for precious metals recovery. *JOM* **59**, 43–47 (2007).
22. Lopes, P. P. et al. Dynamics of electrochemical Pt dissolution at atomic and molecular levels. *J. Electroanal. Chem.* **819**, 123–129 (2018).
23. Lin, W. et al. 'Organic aqua regia'—powerful liquids for dissolving noble metals. *Angew. Chem. Int. Ed.* **49**, 7929–7932 (2010).
24. Hong, Y. et al. Precious metal recovery from electronic waste by a porous porphyrin polymer. *Proc. Natl Acad. Sci. USA* **117**, 16174–16180 (2020).
25. Okesola, B. O., Suravaram, S. K., Parkin, A. & Smith, D. K. Selective extraction and in situ reduction of precious metal salts from model waste to generate hybrid gels with embedded electrocatalytic nanoparticles. *Angew. Chem. Int. Ed.* **55**, 183–187 (2016).
26. Wang, H. et al. Semiconductor heterojunction photocatalysts: design, construction, and photocatalytic performances. *Chem. Soc. Rev.* **43**, 5234–5244 (2014).
27. Cherevko, S. et al. Dissolution of noble metals during oxygen evolution in acidic media. *ChemCatChem* **6**, 2219–2223 (2014).
28. Tian, J. et al. Kinetics on leaching rare earth from the weathered crust elution-deposited rare earth ores with ammonium sulfate solution. *Hydrometallurgy* **101**, 166–170 (2010).
29. Zhou, J. et al. Leaching kinetics of potassium and aluminum from phosphorus-potassium associated ore in HCl-CaF_2 system. *Sep. Purif. Technol.* **253**, 117528 (2020).
30. Dong, C. et al. Size-dependent activity and selectivity of carbon dioxide photocatalytic reduction over platinum nanoparticles. *Nat. Commun.* **9**, 1252 (2018).
31. Sun, C. & Xue, D. In situ IR spectral observation of $NH_4H_2PO_4$ crystallization: structural identification of nucleation and crystal growth. *J. Phys. Chem. C* **117**, 19146–19153 (2013).
32. Ennis, C., Auchettl, R., Ruzi, M. & Robertson, E. G. Infrared characterisation of acetonitrile and propionitrile aerosols under Titan's atmospheric conditions. *Phys. Chem. Chem. Phys.* **19**, 2915–2925 (2017).
33. Yu, H. L. et al. Unidirectional suppression of hydrogen oxidation on oxidized platinum clusters. *Nat. Commun.* **4**, 2500 (2013).
34. Chaudhuri, P. et al. Electronic structure of bis(o-iminobenzosemiquinonato) metal complexes (Cu, Ni, Pd). The art of establishing physical oxidation states in transition-metal complexes containing radical ligands. *J. Am. Chem. Soc.* **123**, 2213–2223 (2001).
35. Siemer, N. et al. Atomic scale explanation of O_2 activation at the Au-TiO_2 interface. *J. Am. Chem. Soc.* **140**, 18082–18092 (2018).
36. Li, R. et al. Radical-involved photosynthesis of AuCN oligomers from Au nanoparticles and acetonitrile. *J. Am. Chem. Soc.* **134**, 18286–18294 (2012).
37. Zheng, Z. et al. Facile in situ synthesis of visible-light plasmonic photocatalysts M@TiO_2 (M = Au, Pt, Ag) and evaluation of their photocatalytic oxidation of benzene to phenol. *J. Mater. Chem.* **21**, 9079–9087 (2011).
38. Bilski, J. et al. Photochemical reactions involved in the phototoxicity of the anticonvulsant and antidepressant drug lamotrigine (Lamictal@). *Photochem. Photobiol.* **85**, 1327–1335 (2009).
39. Han, G. et al. Visible-light-driven valorization of biomass intermediates integrated with H_2 production catalyzed by ultrathin Ni/CdS uanosheets. *J. Am. Chem. Soc.* **139**, 15584–15587 (2017).
40. Hokuto, F. et al. Determining the composite structure of Au-Fe-based submicrometre spherical particles fabricated by pulsed-laser melting in liquid. *Nanomaterials* **9**, 198 (2019).
41. Xiao, J. et al. Integration of plasmonic effects and schottky junctions into metal organic framework composites: steering charge flow for enhanced visible-light photocatalysis. *Angew. Chem. Int. Ed.* **57**, 1103–1107 (2017).
42. Frens, G. Controlled nucleation for the regulation of the particle size in monodisperse gold suspensions. *Nat. Phys. Sci.* **241**, 20–22 (1973).
43. Lee, P. C. & Melsel, D. J. J. Adsorption and surface-enhanced raman of dyes on silver and gold sols. *J. Phys. Chem.* **86**, 3391–3395 (1982).
44. Liu, L., Gao, F. & Zhao, H. Tailoring Cu valence and oxygen vacancy in Cu/TiO_2 catalysts for enhanced CO_2 photoreduction efficiency. *Appl. Catal. B* **134–135**, 349–358 (2013).

Acknowledgements

This work was supported by the National Key Research and Development Program of China (no. 2020YFA0211004), the National Natural Science Foundation of China (nos. 21876114 and 21761142011), Shanghai Government (nos. 19DZ1205102, 19160712900 and 18JC1412900), the Chinese Education Ministry Key Laboratory and International Joint Laboratory on Resource Chemistry, the Shanghai Eastern Scholar Program and the Shanghai Engineering Research Center of Green Energy Chemical Engineering (no. 18DZ2254200).

Author contributions

Y.C., M.X., Z.B. and H.L. conceived the idea for the paper. Y.C. and Z.B. designed the experiments. Y.C., J.W. and Y.W. synthesized the material. Q.Z., Y.D., X.C. and Z.L.W. performed the high-angle annular dark-field STEM imaging. Y.C. performed the sample characterization. Z.B., Z.L.W. and H.L. conducted the experiments. Y.C. and Z.B. analysed the data and wrote the manuscript. All of the authors contributed to writing the paper.

Competing interests

The authors have filed a patent application (US Patent application no. 17042775) on technology related to the processes described in this Article.

Additional information

Supplementary information The online version contains supplementary material available at https://doi.org/10.1038/s41893-021-00697-4.

Correspondence and requests for materials should be addressed to Z.L.W., H.L. or Z.B.

Peer review information *Nature Sustainability* thanks Sheng Dai, Bernd Friedrich and the other, anonymous, reviewer(s) for their contribution to the peer review of this work.

nature research

Corresponding author(s): Zhong Lin Wang, Hexing Li & Zhenfeng Bian

Last updated by author(s): Feb 4, 2021

Reporting Summary

Nature Research wishes to improve the reproducibility of the work that we publish. This form provides structure for consistency and transparency in reporting. For further information on Nature Research policies, see our Editorial Policies and the Editorial Policy Checklist.

Statistics

For all statistical analyses, confirm that the following items are present in the figure legend, table legend, main text, or Methods section.

n/a	Confirmed	
☐	☒	The exact sample size (n) for each experimental group/condition, given as a discrete number and unit of measurement
☐	☒	A statement on whether measurements were taken from distinct samples or whether the same sample was measured repeatedly
☐	☒	The statistical test(s) used AND whether they are one- or two-sided *Only common tests should be described solely by name; describe more complex techniques in the Methods section.*
☐	☒	A description of all covariates tested
☐	☒	A description of any assumptions or corrections, such as tests of normality and adjustment for multiple comparisons
☐	☒	A full description of the statistical parameters including central tendency (e.g. means) or other basic estimates (e.g. regression coefficient) AND variation (e.g. standard deviation) or associated estimates of uncertainty (e.g. confidence intervals)
☐	☒	For null hypothesis testing, the test statistic (e.g. F, t, r) with confidence intervals, effect sizes, degrees of freedom and P value noted *Give P values as exact values whenever suitable.*
☐	☒	For Bayesian analysis, information on the choice of priors and Markov chain Monte Carlo settings
☐	☒	For hierarchical and complex designs, identification of the appropriate level for tests and full reporting of outcomes
☐	☒	Estimates of effect sizes (e.g. Cohen's d, Pearson's r), indicating how they were calculated

Our web collection on statistics for biologists contains articles on many of the points above.

Software and code

Policy information about availability of computer code

Data collection	Gatan DigitalMicrograph (DM) was used as the analysis software of TEM images. XRD analysis software JADE.
Data analysis	Origin 8.6, Microsoft Office 2013

For manuscripts utilizing custom algorithms or software that are central to the research but not yet described in published literature, software must be made available to editors and reviewers. We strongly encourage code deposition in a community repository (e.g. GitHub). See the Nature Research guidelines for submitting code & software for further information.

Data

Policy information about availability of data

All manuscripts must include a data availability statement. This statement should provide the following information, where applicable:
- Accession codes, unique identifiers, or web links for publicly available datasets
- A list of figures that have associated raw data
- A description of any restrictions on data availability

The data that support the findings of this study are available from the corresponding author upon reasonable request.

Field-specific reporting

Please select the one below that is the best fit for your research. If you are not sure, read the appropriate sections before making your selection.

☐ Life sciences ☐ Behavioural & social sciences ☒ Ecological, evolutionary & environmental sciences

For a reference copy of the document with all sections, see nature.com/documents/nr-reporting-summary-flat.pdf

Ecological, evolutionary & environmental sciences study design

All studies must disclose on these points even when the disclosure is negative.

Study description	We show a photocatalytic process that allows one to subversively retrieve precious metals from circuit boards, ternary automotive catalysts and even ores in an environmentally friendly, scalable and efficient manner by using TiO2 or other photocatalysts.
Research sample	Circuit boards, Ternary automotive catalysts and even ores
Sampling strategy	Central Processing Unit (CPU), ore and three-way catalyst (TWC) were purchased from Alibaba (Shanghai, China). All the chemicals were used as received.
Data collection	Experiment in the laboratory.
Timing and spatial scale	From June 2017 to December 2020, each group of data shall be repeated at least three times
Data exclusions	No data were excluded from the analyses
Reproducibility	All attempts to repeat the experiment were successful
Randomization	No data were excluded from the analyses
Blinding	Data collection by different person in different time periods

Did the study involve field work? ☐ Yes ☒ No

Reporting for specific materials, systems and methods

We require information from authors about some types of materials, experimental systems and methods used in many studies. Here, indicate whether each material, system or method listed is relevant to your study. If you are not sure if a list item applies to your research, read the appropriate section before selecting a response.

Materials & experimental systems

n/a	Involved in the study	
☒	☐	Antibodies
☒	☐	Eukaryotic cell lines
☒	☐	Palaeontology and archaeology
☒	☐	Animals and other organisms
☒	☐	Human research participants
☒	☐	Clinical data
☒	☐	Dual use research of concern

Methods

n/a	Involved in the study	
☒	☐	ChIP-seq
☒	☐	Flow cytometry
☒	☐	MRI-based neuroimaging